Characterization of the microstructure of spin-coated and blade coated all-polymer solar cells

Chao Wang,[a] Amelia C. Y. Liu,[b] Martyn Jevric,[c] Jonas M. Bjuggren,[c] Mats R. Andersson,[c] and Christopher R. McNeill[b]

[a] *Materials Science and Engineering, Monash University, Wellington Road, Clayton, VIC 3800, Australia*

[b] *Monash Centre for Electron Microscopy, and School of Physics and Astronomy, Monash University, Wellington Road, Clayton, Victoria 3800, Australia*

[c] *Flinders Centre for Nanoscale Science and Technology, Flinders University, Sturt Road, Bedford Park, Adelaide, SA 5042, Australia*

24th June 2019

Key words: All-polymer solar cells, morphology, microstructure, GIWAXS, AFM, TEM.

Summary of Key Findings

The microstructure of six all-polymer blends is examined. J52 is used as the donor, paired with 6 acceptor polymers derived from the N2200 structure. In addition to N2200, F-N2200, PNDIT10 and three new acceptor polymers developed at Flinders University employed. Atomic force microscopy (AFM), transmission electron microscopy (TEM) and synchrotron-based grazing-incidence wide-angle X-ray scattering (GIWAXS) are employed to study thin film topography, bulk morphology and thin film microstructure respectively. All blends studied were found to exhibit a fine intermixing between donor and acceptor which should be supportive of efficient solar cell operation. The microstructure of both spin-coated and blade-coated films are studied. Good correspondence between spin-coated and blade-coated microstructures is found demonstrating that all-polymer microstructure is relatively robust to coating method.

Introduction

All-polymer solar cells have active layers based on blends of two semiconducting polymers.[1] With a view to commercialisation, all-polymer solar cells have a number of potential advantages over other organic PV technologies including improved morphological stability.[2] The fact that two polymers are blended together means that an all-polymer blend, as distinct to a blend based on a semiconducting donor polymer and small molecule acceptor, has a lower tendency to phase segregate due to the entanglement of polymer chains rendering them with a low physical mobility.[3, 4] The blending of two polymers can be challenging to produce an optimum nanoscale morphology as required for the efficient operation of a bulk heterojunction solar cell.[4] As tightly bound excitons – which are the primary product of photoexcitation in organic semiconductors – can only diffuse around 10 nm or less before they recombine,[5] donor and acceptor materials must be intermixed such that there are donor/acceptor heterojunctions within 10 nm of exciton generation to ensure that excitons are dissociated into electron-hole pairs at the donor/acceptor interface before they recombine.[4] The long chains of semiconducting polymers means that there can be a tendency for all-polymer blends to phase separate into mesoscale domains (with domain size much larger than the exciton diffusion length) due to the reduced entropy of mixing of two polymers compared to a polymer and small molecule.[4] Furthermore, the extended nature of polymer chains means that polymer chains begin to interact earlier in the solution coating process potentially initiating phase separation earlier in the film drying process.

While active layer films in the laboratory are generally prepared via spin-coating, the commercial production of polymer solar cells will rely on in-line or roll-to-roll coating processes.[6] Due to the different kinetics of drying in a small spin-coating vs. a large area coating process, the morphologies produced via spin-coating may not be reproduced when device production is scaled up.[7] As a lab-based alternative to spin-coating, blade coating can enable the fabrication of test-size devices minimising material wastage for device optimisation, with drying kinetics comparable to roll-to-roll coating enabling.[8] Thus the efficiencies and morphologies realised in small area blade-coated cells can be more directly transferred to large area cells produced via commercially relevant processes. In this report the efficiency and morphology of all-polymer solar cells produced via spin-coating and via blade coating are directly compared. Six different all-polymer systems are compared, including 3 not previously reported. Microstructure is characterised using a combination of atomic force microscopy (AFM), transmission electron microscopy (TEM) and synchrotron-based grazing-incidence wide-angle X-ray scattering (GIWAXS). These three techniques provide a comprehensive overview of surface roughness and topography (AFM), bulk phase separation and morphology (TEM) and thin film crystallinity (GIWAXS).

Methodology

Materials

For all blends the donor polymer J52 was employed.[9] This donor was chosen due to the high efficiency that can be achieved in all-polymer solar cells with this donor when combined with suitable acceptors,[10] and due to the superior stability compared to traditional donors such as PTB7-Th. As acceptor polymers, six NDI-based acceptors were used, including previously reported N2200,[11] F-N2200,[12] PNDI-T10[13] along with three new polymers MJA109, MJA185 and MJA199. The chemical structures of these polymers are shown in figure 1. J52 and F-N2200 were sourced commercially from 1-Material Inc. N2200 was sourced commercially from Raynergy Tek. Inc. PDNI-T10, MJA109, MAJ185 and MJA199 were synthesized in-house at Flinders University.

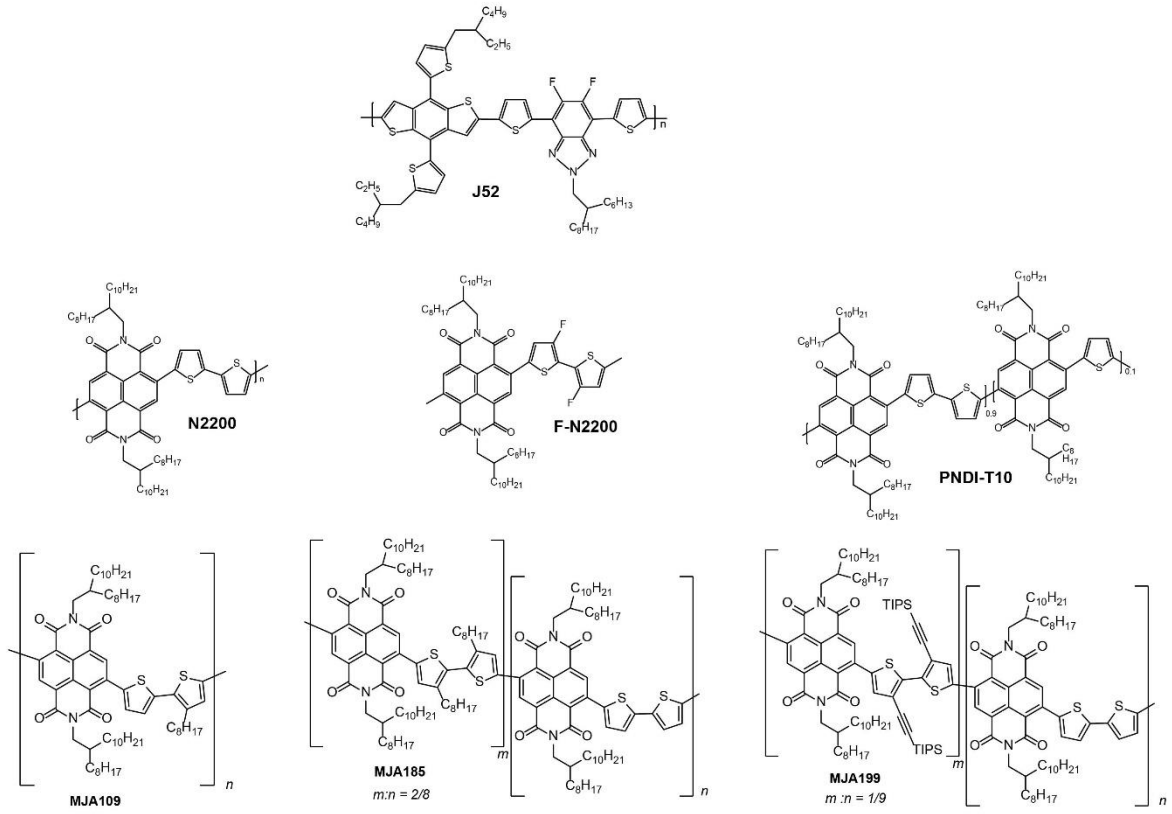

Figure 1. Chemical structures of polymers studied.

Sample preparation

Spin-coating was performed with a Laurell WS-650Mz-23NPPB spin-processor. The active layers of spin-coated solar cells were prepared from blend solutions at different spin speed for 60 s to optimise film thickness. Blade coating was performed using a home-built blade coater based on the system developed at NIST.[14] For blade-coated devices, the active layers were blade-coated with different coating speed in order to optimise film thickness. Samples for microstructure measurement were prepared in such a way to match films in devices as closely as possible. For AFM and GIWAXS measurements, films were coated on PEIE-coated substrates (either glass or silicon) using the same deposition conditions used in devices. For TEM, films were coated onto substrates with a thick, unannealed PEIE layer to mimic the surface energy of devices and facilitate floating off onto copper TEM grids.

Transmission electron microscopy

Transmission electron microscopy (TEM) images were obtained using a JEOL JEM-2100F transmission electron microscope operating at a voltage of 200 kV. Defocused bright-field images were collected using a Gatan UltraScan 1000 (2k × 2k) CCD camera. A 20 µm objective aperture and a large defocus value of −10 000 nm were used to increase contrast between the phases.

Atomic force microscopy

Atomic force microscopy (AFM) images were performed at the Melbourne Centre for Nanofabrication using a Bruker Dimension Icon in ScanAsyst mode.

Grazing incidence wide-angle X-ray scattering

GIWAXS measurements were performed at the SAXS/WAXS beamline at the Australian Synchrotron.[15] An in-vacuum Dectris PILATUS3 X 2M detector was used to record scattering patterns from 15 keV X-rays. Background signal from the substrate scatter was minimized by keeping the incident angle of the X-ray beam close to the critical angle of the polymer film but below the critical angle of the substrate. Damage to the film was avoided by limiting the X-ray exposure time to 3 s. The sample-to-detector distance was calibrated using a silver behenate sample. The results were analyzed by an altered version of the NIKA 2D data reduction package implemented in IgorPro.[16] Further details can be found elsewhere.[17]

Results

Atomic force microscopy and transmission electron microscopy

The AFM surface topography (a, c, e, f, g, I, k) and TEM micrographs (b, d, f, h, j, l) for spin coated blend films and blade coated films are shown in figure 2 and figure 3 separately. In general, relatively smooth and intimately mixed morphologies are observed, different to mesoscale morphologies that have limited the efficiency of earlier all-polymer blends.[4] The contrast that is seem in the TEM images reflects features that are seen in AFM suggesting that this TEM contrast is due to thickness variation rather than internal structure, with TEM unable to discern coarse phase separation on a length scale larger than 50 nm. Comparing blade coated and spin-coated samples, blade-coated samples in general have smoother surfaces as evidenced by the calculated root man square (R_q) roughness values, see values in table 1. The only exception is that of the J52:F-N2200 system that has a surface roughness value of 0.91 nm for the spin-coated sample compared to 1.38 nm for the blade-coated sample. The spin-coated J52:MJA185 film has the highest surface roughness (4.04 nm) while the blade-coated J52:N2200 system has the smallest surface roughness (0.83 nm). Although the J52:N2200 system in general shows a smooth surface topography, there appear to be undissolved N2200 particles in the film which appear as dark spots in the TEM images.

Table 1. Summary of film preparation conditions and surface roughness values for the six systems studied.

System	Weight ratio	Solvent	Spin-coated R_q (nm)	Blade-coated R_q (nm)
J52:N2200	1:1	Chlorobenzene	1.38	0.83
J52:F-N2200	1:1	Chlorobenzene	0.91	1.38
J52:PNDIT10	1:1	Chlorobenzene	2.29	1.11
J52:MJA109	1:1	Chlorobenzene	2.01	1.19
J52:MJA185	1:1	Chlorobenzene	4.04	1.40
J52:MJA199	1:1	Chlorobenzene	2.36	1.63

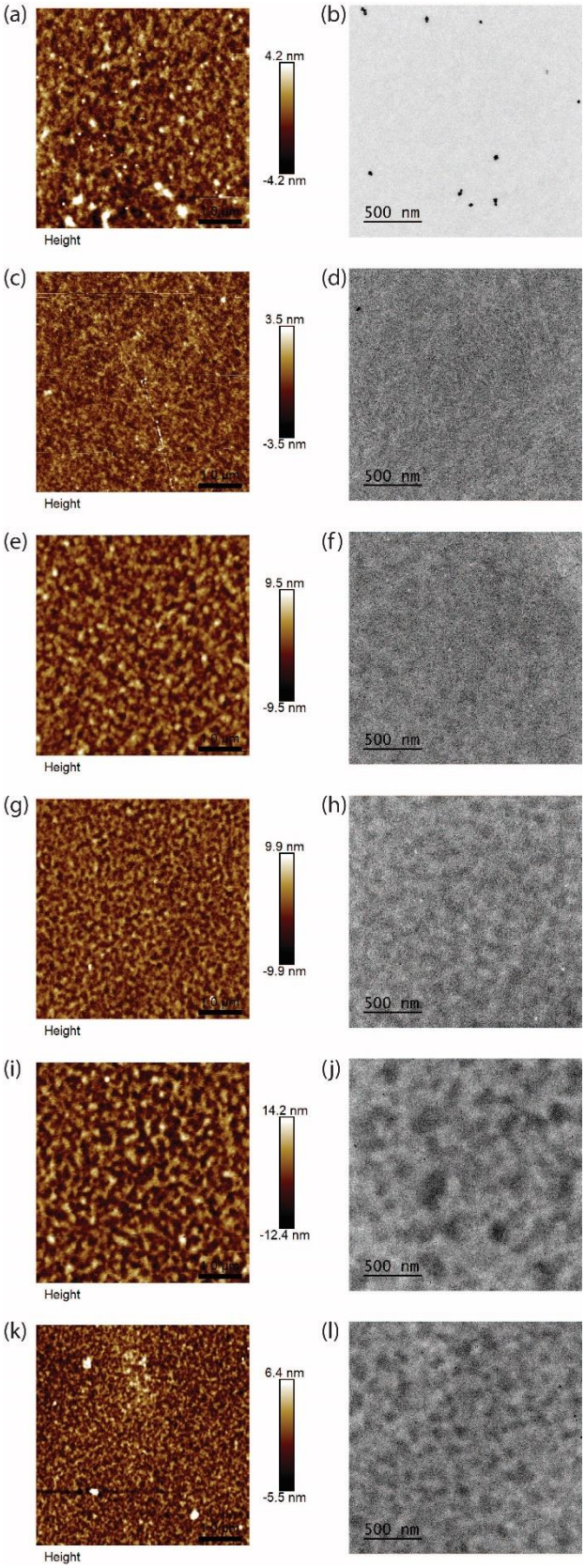

Figure 2. AFM (a, c, e, g, i, k) and TEM images (b, d, f, h, j, l) of the spin coated J52:N2200 blend (a, b), J52:F-N2200 blend (c, d), J52:PNDI-T10 38K blend (e, f), J52: MJA199 blend (g, h), J52: MJA185 blend (i, j), J52:MJA109 blend (k, l).

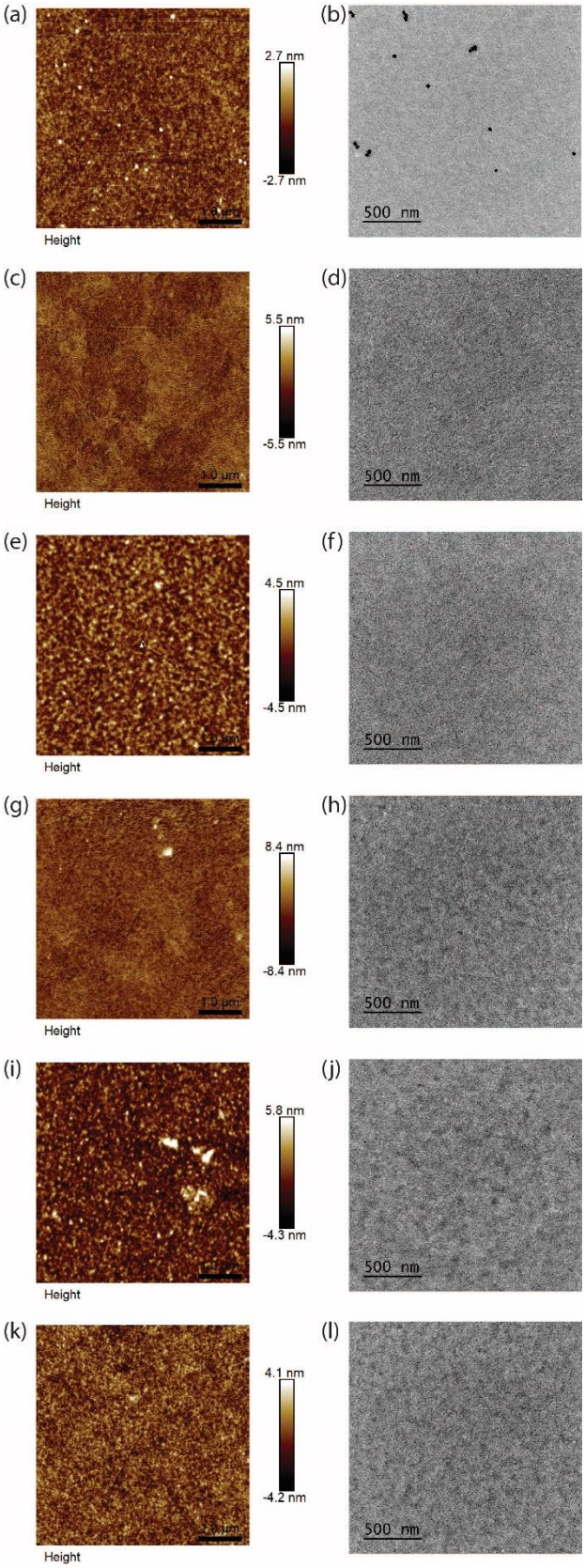

Figure 3. AFM (a, c, e, g, i, k) and TEM images (b, d, f, h, j, l) of the spin coated J52:N2200 blend (a, b), J52:F-N2200 blend (c, d), J52:PNDI-T10 38K blend (e, f), J52: MJA199 blend (g, h), J52: MJA185 blend (i, j), J52:MJA109 blend (k, l).

Grazing incidence wide-angle X-ray scattering

Before studying the scattering patterns of blend films, the GIWAXS results of neat films are considered first. Figure 4 presents the 2D scattering patterns and 1D line scattering line profiles along in-plane and out-of-plane directions. All neat samples exhibit a semicrystalline microstructure characterised by a alkyl stacking peak located at ~ 2.5 $Å^{-1}$ to 3.0 $Å^{-1}$ and a π-π stacking peak at 16 to 18 $Å^{-1}$. For all samples a "face-on" packing of polymer chains is observed with alkyl stacking peaks appearing predominantly along the in-plane scattering direction and π-π stacking peaks appearing predominately along the out-of-plan scattering direction. The donor polymer, J52, exhibits a relatively low degree of crystalline order evidenced weak scattering features, a lack of higher order reflections and large spread of crystal plane orientations. J52 also has a distinct alkyl stacking peak at a value of ~ 3.0 $Å^{-1}$ which is large than that of the acceptor polymers which have an alkyl stacking peak at ~ 2.5 $Å^{-1}$. This difference in alkyl stacking peak locations between J52 and acceptors is consistent with the shorter alkyl chain length for J52 compared to the N2200-derived polymers. The π-π stacking peak of J52 also appears at a larger q-spacing, at around 18 $Å^{-1}$ compared to a value of 16.5 $Å^{-1}$ to 17.0 $Å^{-1}$ for the acceptor polymers. Of the acceptor polymers, N2200 is the most ordered evidenced by sharper alkyl stacking reflections, higher order reflections and well-defined back-bone reflections, features consistent with previous reports.[18, 19] F-N2200 also shows a relatively high degree of order, albeit with broader alkyl stacking reflections. The other acceptor polymers exhibit weaker scattering features, consistent with the introduction of different monomer units to disrupt molecular packing. Interestingly MJA199 still exhibits a relatively high degree of order (although still lower than that of N2200) despite the introduction of monomer units with bulky TIPS groups.

The GIWAXS results of spin-coated and blade-coated samples are shown in figures 5 through 10. In general the scattering patterns of the blend films can be regarded as showing scattering features from both donor and acceptor, though the scattering from the acceptor polymer dominate the features due to high degree of order of the acceptor material. Scattering features in the blend are broader due to overlapping alkyl stacking and π-π stacking peaks. The polymers retain a similar face-on orientation in the blends. The acceptor polymers with stronger scattering features are also found to exhibit stronger scattering features in the blend with J52. These observations show that in all these blends, both donor and acceptor crystallise.

The comparison between spin-coated and blade-coated films provides an opportunity to assess the influence of coating process on thin film microstructure. Comparing the GIWAXS data for spin-coated and blade-coated samples, a very similar microstructure is observed. Indeed the scattering patterns and profiles are near identical; there are some differences in the absolute scattering intensities however these are due to differences in film thickness.

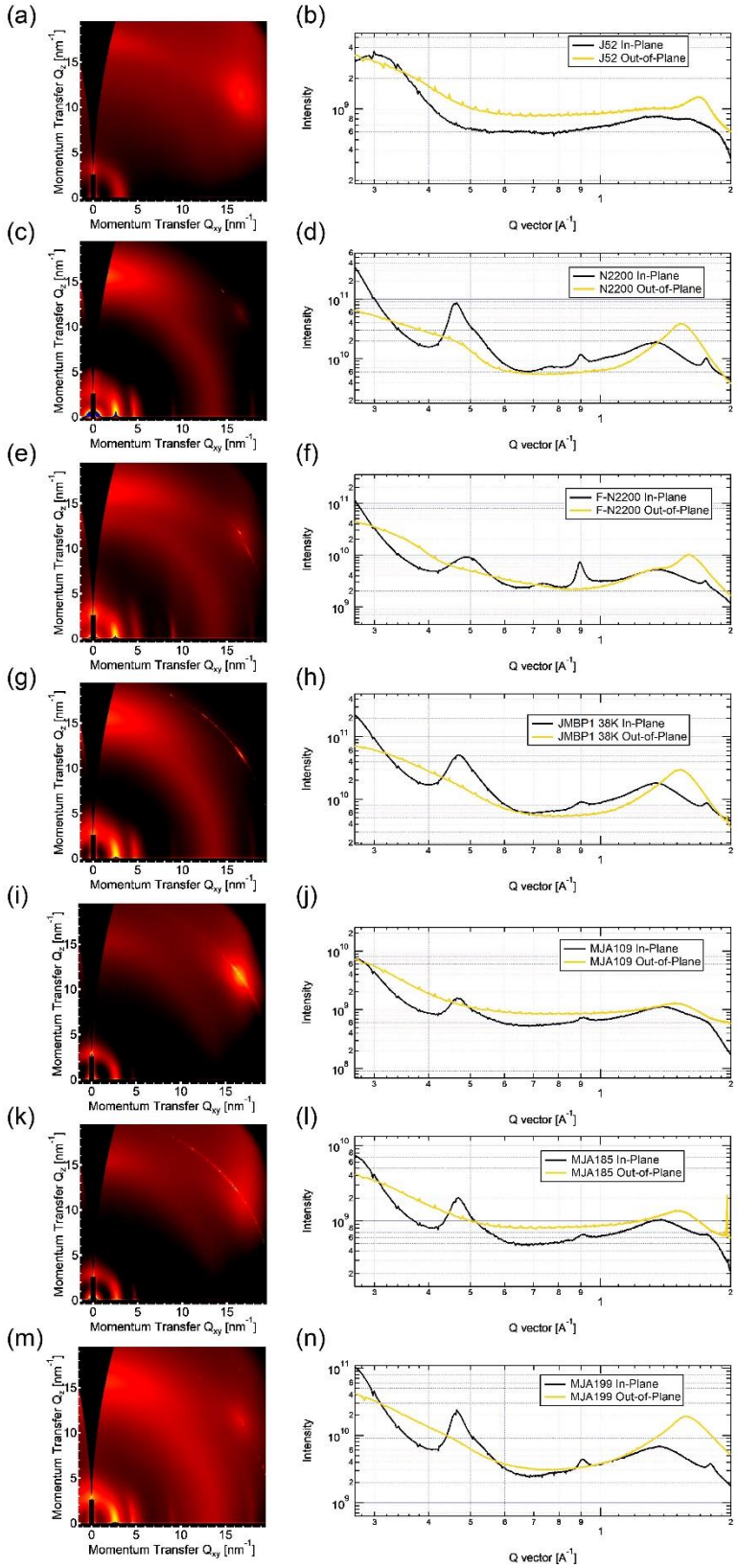

Figure 4. GIWAXS data of neat films. (a, c, e, g, i, k, m) show the 2D scattering patterns while (b, d, f, h, j, l, n) show ID line profiles taken along in-plane and out-of-plane directions. (a, b) show data for J52; (c, d) show data for N2200; (e, f) show data for F-N2200; (g, h) show data for PNDIT10 (JMBP1); (i, j) show data for MJA109; (k, l) show data for MJA185; (m, n) show data for MJA199.

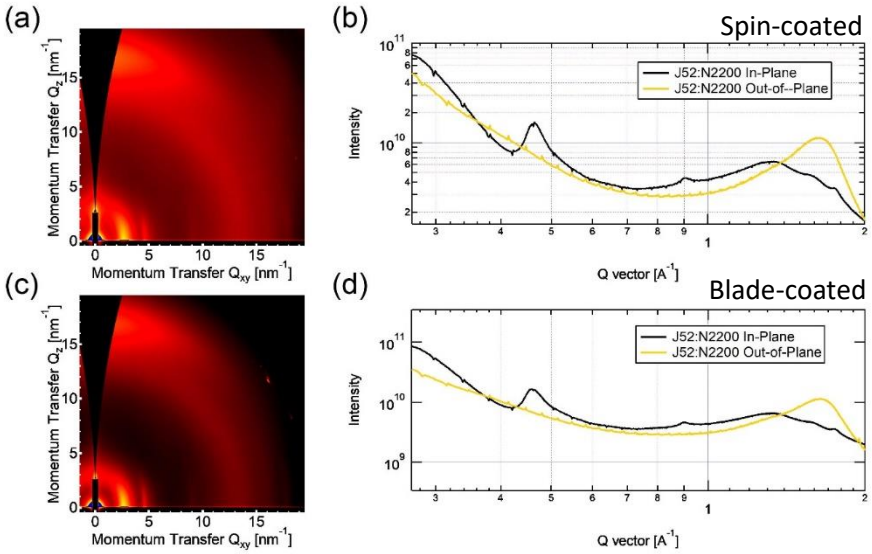

Figure 5. GIWAXS data of the J52:N2200 blend. (a, b) are of the spin-coated film while (c, d) are of the blade-coated film.

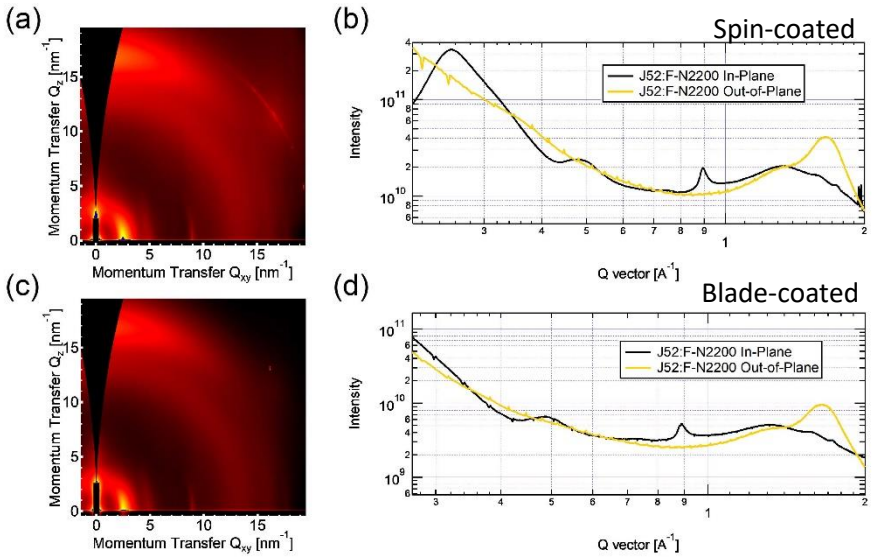

Figure 6. GIWAXS data of the J52:F-N2200 blend. (a, b) are of the spin-coated film while (c, d) are of the blade-coated film.

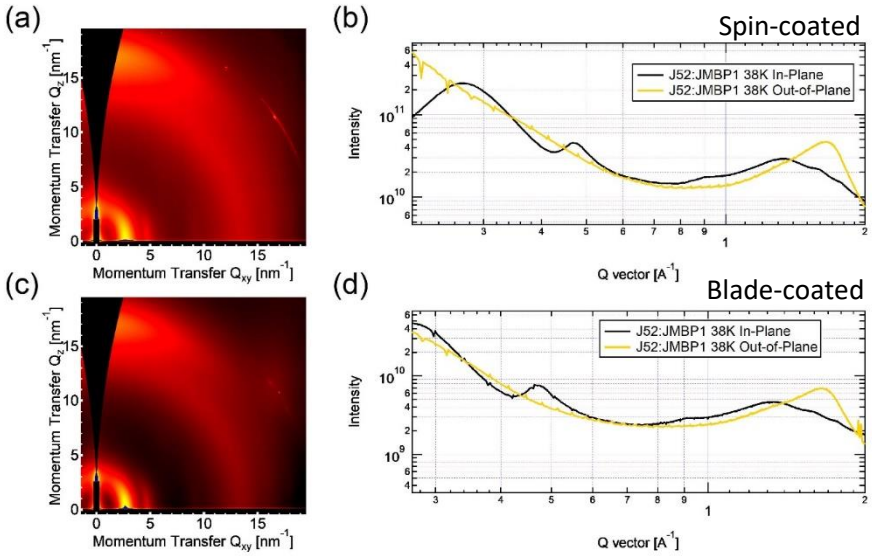

Figure 7. GIWAXS data of the J52:PNDIT10 blend. (a, b) are of the spin-coated film while (c, d) are of the blade-coated film.

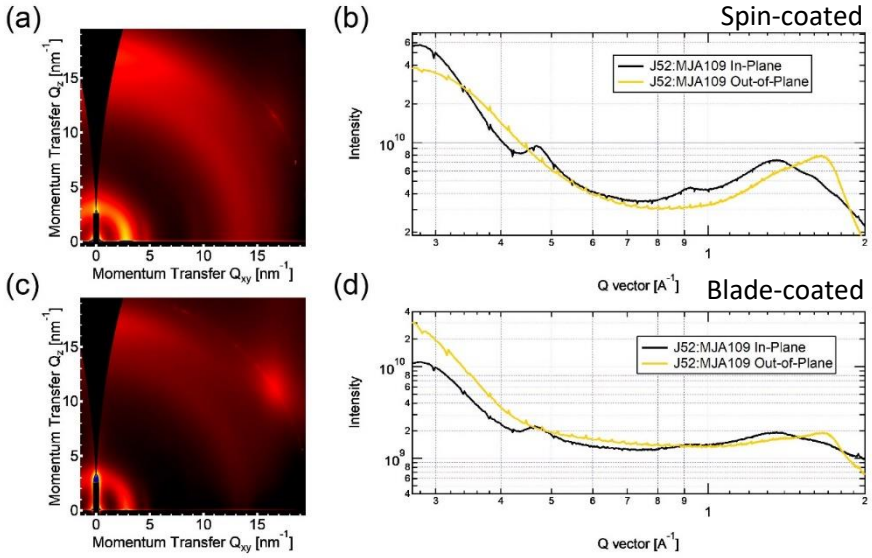

Figure 8. GIWAXS data of the J52:MJA109 blend. (a, b) are of the spin-coated film while (c, d) are of the blade-coated film.

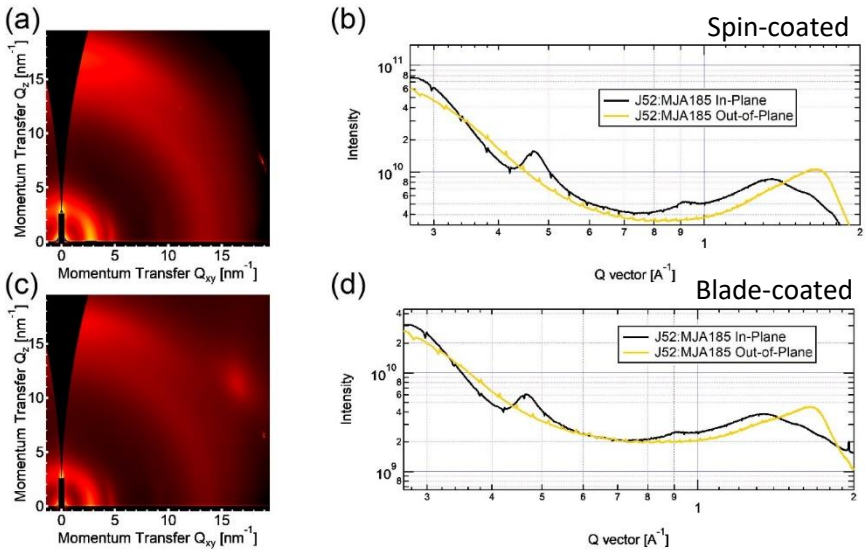

Figure 9. GIWAXS data of the J52:MJA185 blend. (a, b) are of the spin-coated film while (c, d) are of the blade-coated film.

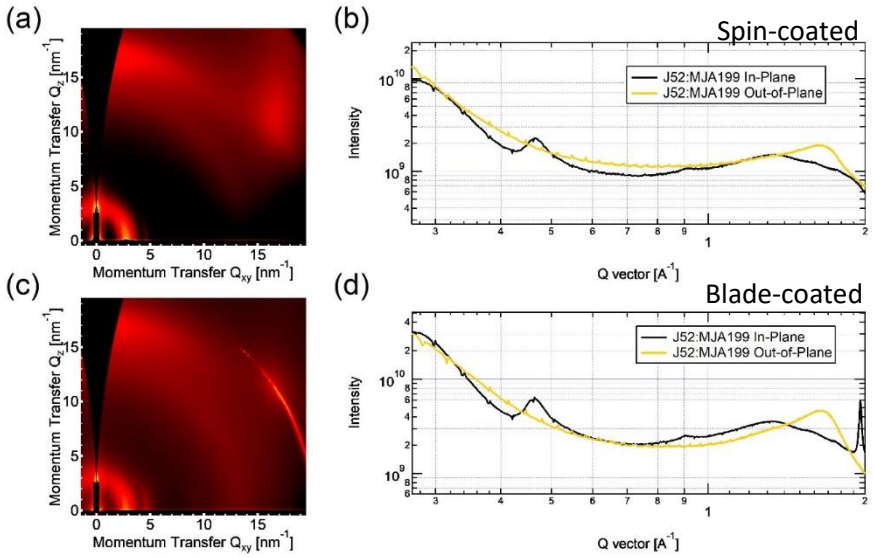

Figure 10. GIWAXS data of the J52:MJA199 blend. (a, b) are of the spin-coated film while (c, d) are of the blade-coated film

Conclusions

This report has examined the microstructure of six all-polymer blends, based on six different acceptor polymers pair with the donor polymer J52. As well as the acceptor polymers N2200, F-N2200, and PNDIT10, blends of J52 with three new acceptor polymers (MJA109, MJA185, and MJA199) have been investigated. From AFM and TEM analysis, all blends show a fine intermixing of donor and acceptor. Blade coated films were found to exhibit smoother surface roughness values in general. From the GIWAXS analysis, both spin-coated and blade-coated films show near identical microstructures. Variations in the degree of crystalline order for the different acceptor polymers was evident, consistent with the varying in chemical structure to tune crystallinity. The microstructure of the blends reflected that of the neat films. The good correspondence between spin-coated and blade-coated microstructures demonstrates that all-polymer microstructure is relatively robust to coating method.

Acknowledgements

This Activity received funding from ARENA as part of ARENA's Research and Development Program – Solar PV Research, project number 2017/RND0014, “Bringing All-Polymer Solar Cells Closer to Commercialization.” The views expressed herein are not necessarily the views of the Australian Government, and the Australian Government does not accept responsibility for any information or advice contained herein. This work was performed in part at the SAXS/WAXS and soft X-ray beamlines at the Australian Synchrotron, part of ANSTO. This work was also performed in part at the Melbourne Centre for Nanofabrication (MCN) in the Victorian Node of the Australian National Fabrication Facility. The authors acknowledge the use of facilities within the Monash Centre for Electron Microscopy.

References

1. McNeill, C. R.; Greenham, N. C., Conjugated-Polymer Blends for Optoelectronics. *Adv. Mater.* **2009,** 21, 3840 - 3850.
2. Wang, G.; Melkonyan, F. S.; Facchetti, A.; Marks, T. J., All-Polymer Solar Cells: Recent Progress, Challenges, and Prospects. *Angewandte Chemie International Edition* **2019,** 58, 4129-4142.
3. Kim, T.; Choi, J.; Kim, H. J.; Lee, W.; Kim, B. J., Comparative Study of Thermal Stability, Morphology, and Performance of All-Polymer, Fullerene–Polymer, and Ternary Blend Solar Cells Based on the Same Polymer Donor. *Macromolecules* **2017**, DOI: 10.1021/acs.macromol.7b00834.
4. McNeill, C. R., Morphology of all-polymer solar cells. *Energy & Environ. Sci.* **2012,** 5, 5653-5567.
5. Blom, P. W. M.; Mihailetchi, V. D.; Koster, L. J. A.; Markov, D. E., Device Physics of Polymer:Fullerene Bulk Heterojunction Solar Cells. *Adv. Mater.* **2007,** 19, 1551-1566.
6. Krebs, F. C.; Tromholt, T.; Jørgensen, M., Upscaling of polymer solar cell fabrication using full roll-to-roll processing. *Nanoscale* **2010,** 2, 873-886.
7. Ro, H. W.; Downing, J. M.; Engmann, S.; Herzing, A. A.; DeLongchamp, D. M.; Richter, L. J.; Mukherjee, S.; Ade, H.; Abdelsamie, M.; Jagadamma, L. K.; Amassian, A.; Liu, Y.; Yan, H., Morphology changes upon scaling a high-efficiency, solution-processed solar cell. *Energy & Environ. Sci.* **2016,** 9, 2835-2846.
8. Krebs, F. C., Fabrication and processing of polymer solar cells: A review of printing and coating techniques. *Solar Energy Materials and Solar Cells* **2009,** 93, 394-412.
9. Bin, H.; Zhang, Z.-G.; Gao, L.; Chen, S.; Zhong, L.; Xue, L.; Yang, C.; Li, Y., Non-Fullerene Polymer Solar Cells Based on Alkylthio and Fluorine Substituted 2D-Conjugated Polymers Reach 9.5% Efficiency. *Journal of the American Chemical Society* **2016,** 138, 4657-4664.

10. Huang, W.; Li, M.; Lin, F.; Wu, Y.; Ke, Z.; Zhang, X.; Ma, R.; Yang, T.; Ma, W.; Liang, Y., Rational design of conjugated side chains for high-performance all-polymer solar cells. *Mol. Syst. Des. Eng.* **2018,** 3, 103-112.
11. Yan, H.; Chen, Z.; Zheng, Y.; Newman, C.; Quinn, J. R.; Dötz, F.; Kastler, M.; Facchetti, A., A high-mobility electron-transporting polymer for printed transistors. *Nature* **2009,** 457, 679 - 687.
12. Xu, X.; Li, Z.; Wang, J.; Lin, B.; Ma, W.; Xia, Y.; Andersson, M. R.; Janssen, R. A. J.; Wang, E., High-performance all-polymer solar cells based on fluorinated naphthalene diimide acceptor polymers with fine-tuned crystallinity and enhanced dielectric constants. *Nano Energy* **2018,** 45, 368-379.
13. Li, Z.; Xu, X.; Zhang, W.; Meng, X.; Ma, W.; Yartsev, A.; Inganäs, O.; Andersson, M. R.; Janssen, R. A. J.; Wang, E., High Performance All-Polymer Solar Cells by Synergistic Effects of Fine-Tuned Crystallinity and Solvent Annealing. *J. Am. Chem. Soc.* **2016,** 138, 10935-10944.
14. Stafford, C. M.; Roskov, K. E.; Epps, T. H.; III; Fasolka, M. J., Generating thickness gradients of thin polymer films via flow coating. *Rev. Sci. Instrum.* **2006,** 77, 023908.
15. Kirby, N. M.; Mudie, S. T.; Hawley, A. M.; Cookson, D. J.; Mertens, H. D. T.; Cowieson, N.; Samardzic-Boban, V., A low-background-intensity focusing small-angle X-ray scattering undulator beamline. *J. Appl. Cryst.* **2013,** 46, 1670-1680.
16. Ilavsky, I., Nika - software for 2D data reduction. *J. Appl. Cryst.* **2012,** 45, 324-328.
17. Gann, E.; Caironi, M.; Noh, Y.-Y.; Kim, Y.-H.; McNeill, C. R., Diffractive X-ray Waveguiding Reveals Orthogonal Crystalline Stratification in Conjugated Polymer Thin Films. *Macromolecules* **2018,** 51, 2979-2987.
18. Rivnay, J.; Toney, M. F.; Zheng, Y.; Kauvar, I. V.; Chen, Z.; Wagner, V.; Facchetti, A.; Salleo, A., Unconventional Face-On Texture and Exceptional In-Plane Order of a High Mobility n-Type Polymer. *Adv. Mater.* **2010,** 22, 4359-4363.
19. Schuettfort, T.; Huettner, S.; Lilliu, S.; Macdonald, J. E.; Thomsen, L.; McNeill, C. R., Surface and bulk structural characterization of a high-mobility electron-transporting polymer. *Macromolecules* **2011,** 44, 1530-1539.